Materials Research Express

PAPER • **OPEN ACCESS**

Hot filament chemical vapor deposition temperature field optimization for diamond films deposited on silicon nitride substrates

To cite this article: Yuhou Wu *et al* 2021 *Mater. Res. Express* **8** 116403

View the article online for updates and enhancements.

You may also like

- The Design of Large-aperture HFCVD Diamond-coated Drawing Die Preparation System and Experimental Study on Its Application
Shanxiang Fang, Qinjian Zhang and Shizhe Ji
- Hot-Filament Chemical Vapor Deposition of Organosilicon Thin Films from Hexamethylcyclotrisiloxane and Octamethylcyclotetrasiloxane
Hilton G. Pryce Lewis, Thomas B. Casserly and Karen K. Gleason
- Syntheses of single- and double-wall carbon nanotubes by the HTPAD and HFCVD methods
Toshiki Sugai, Toshiya Okazaki, Hiromichi Yoshida et al.

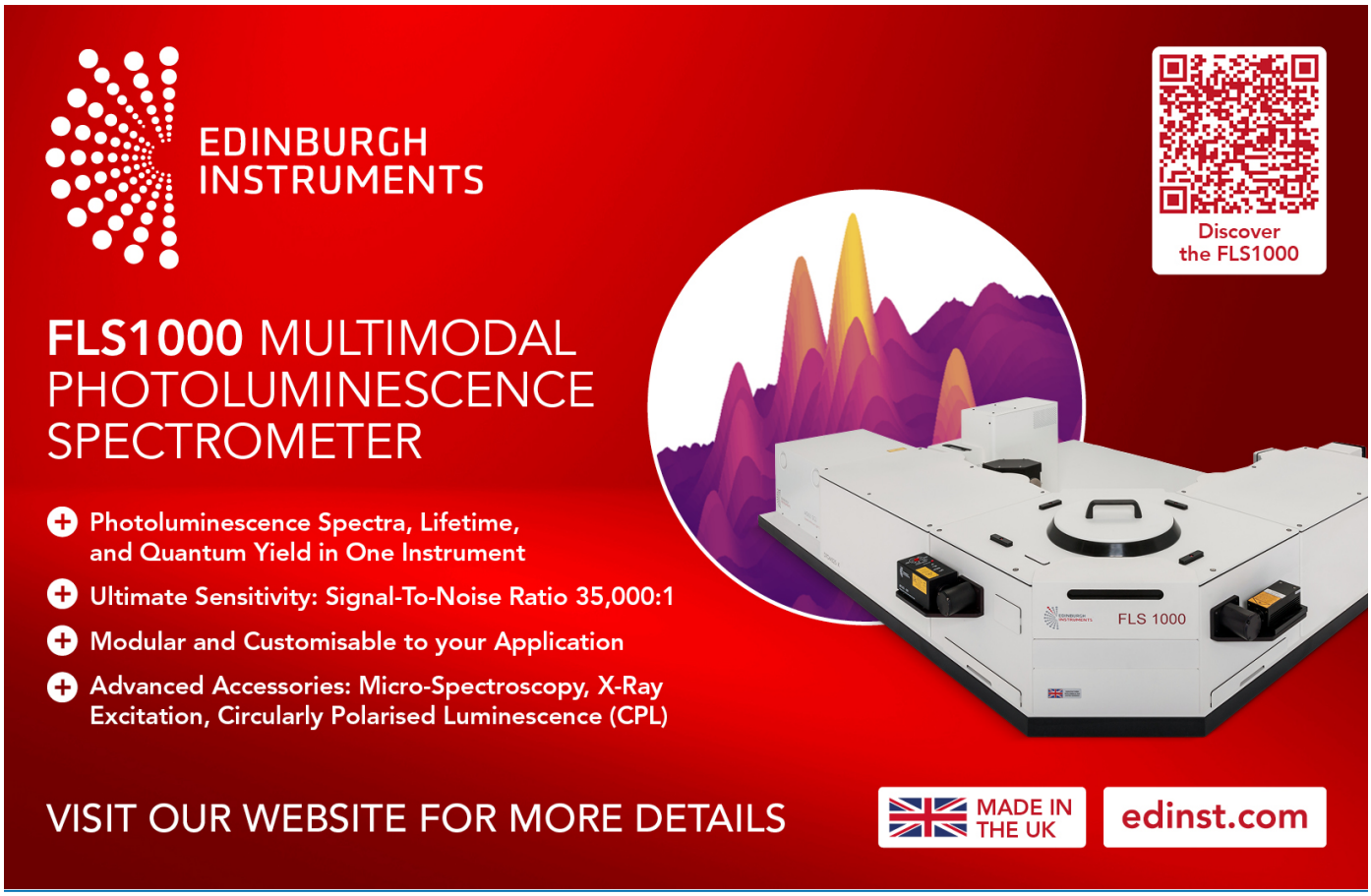

Materials Research Express

PAPER

Hot filament chemical vapor deposition temperature field optimization for diamond films deposited on silicon nitride substrates

Yuhou Wu[1], **Huisen Zhang**[1,2], **Guangyu Yan**[1,2,*], **Lusheng Liu**[3], **Daniel Cristea**[4], **He Wang**[1,2], **Yumiao Yang**[1,2] **and Jianhui Shen**[1,2]

[1] Joint International Research Laboratory of Modern Construction Engineering Equipment and Technology, Shenyang Jianzhu University, 110168 Shenyang, People's Republic of China
[2] School of Mechanical Engineering, Shenyang Jianzhu University, 110168 Shenyang, People's Republic of China
[3] Shenyang National Laboratory for Materials Science, Institute of Metal Research, Chinese Academy of Sciences, 110016 Shenyang, People's Republic of China
[4] Materials Science and Engineering Faculty, Transilvania University, 500036 Brasov, Romania
[*] Author to whom any correspondence should be addressed.

E-mail: ygy0813@sjzu.edu.cn

Keywords: HFCVD, Si3N4 ceramics, diamond film, numerical simulation

OPEN ACCESS

RECEIVED
25 August 2021

REVISED
14 October 2021

ACCEPTED FOR PUBLICATION
22 October 2021

PUBLISHED
11 November 2021

Abstract

The influence of some key parameters of hot filament chemical vapor deposition (HFCVD) on the temperature distribution during the deposition of diamond coatings on silicon nitride (Si_3N_4) substrates was assessed with the help of the finite element method. Solid heat transfer, fluid heat transfer and surface radiation heat transfer mechanisms were used to calculate the substrate temperature in the steady state during the deposition process. The accuracy of the model was verified by comparing the simulation model with experimental measurements. The comparison shows that the deviation between the model and the actual substrate temperature measurements is within 3%. Furthermore, a Taguchi orthogonal experiment was designed (3 factors, 3 levels, L9). By changing the number of hot filaments, the distance between the filaments and the substrate, and the separation between two adjacent hot filaments, the influence trend of these parameters on the substrate temperature was assessed, leading to an optimal hot filament arrangement. A deposition experiment was carried out using the optimized parameters, and the results showed that the substrate surface temperature obtained by numerical simulation is highly consistent with the temperature measured by the infrared thermometer. The optimized deposition parameters contributed to a more suitable temperature range and more uniform temperature distribution on the Si_3N_4 ceramic substrate. The deposited diamond film exhibited uniform crystal quality and grain morphology, thus verifying the validity of the simulation results.

1. Introduction

Diamond films deposited by chemical vapor deposition (CVD) exhibit excellent properties such as high hardness, high elastic modulus, extremely high thermal conductivity, good self-lubricity and chemical inertness, which are very close to natural diamond. Diamond films are being widely used on various structural parts as wear-resistant protective coatings under extreme conditions such as high temperature, strong corrosion and high pressure [1–4]. Si_3N_4 ceramics have been selected as a substrate duo to their low thermal mismatch and good chemical compatibility with diamond, resulting in significantly enhanced diamond-substrate adhesion. In addition, the high hardness and excellent thermal shock resistance of Si_3N_4 also make it a more than adequate option as a substrate material for diamond coatings [5–8].

Among the current methods for preparing diamond films, hot filament chemical vapor deposition (HFCVD) has attracted widespread attention, due to its relative simplicity and low cost, and the possibility to

coat large-area and large-scale structural parts [9–11]. The bonding reaction between hydrocarbon groups and carbon atoms used to form diamond films during vapor deposition often occurs on the surface of the substrates [12, 13]. Therefore, the substrate temperature distribution during deposition largely determines the quality of diamond films. During the production of multiple diamond-coated parts in the same batch, the diamond grain size and film-substrate adhesion caused by uneven heating of the substrate are usually nonuniform. Therefore, the deposition process should be optimized by studying the comprehensive influence of various parameters on the substrate temperature. In previous studies [14, 15], most simulations focused on the physical field of radiation heat transfer, without assessing the influence of non-isothermal flow on the temperature distribution of the substrate, which leads to a large deviation after solving the model. Song *et al* [16] studied the influence of the deposition parameters of diamond films prepared by HFCVD, showing that the highest growth rate and the best film quality are obtained when the filament is heated to 2715 K and the substrate is heated to 1161 K. Moreover, Wang *et al* [17] used the finite volume method to study the substrate temperature during the diamond film growth process, and optimized the temperature influence of the substrate by changing the cooling conditions, filament temperature, and filament diameter. Furthermore, Shen *et al* [18] studied the influence of the filament arrangement and the length of the filament on the substrate temperature, and found that the length of the filament and the distance between the filament and the substrate have a significant influence on the substrate temperature field. Zhang *et al* [19] used the finite volume method to simulate the temperature and gas density field distribution inside the hot filament chemical vapor deposition chamber, and studied the influence of the hot filament arrangement and gas inlet position. However, the existence of nonlinear control conditions in the thermal contact boundary was not considered in previous numerical simulation models, which results in a missing influence of contact thermal resistance between two materials on the heat flux. In addition, in order to simplify the model, the material properties of the model such as thermal conductivity, heat capacity and density were set as constants, and the influence of the temperature gradient on the material properties was ignored. For example, the thermal conductivity and heat capacity of the non-isothermal area of hydrogen in the chamber are different. Therefore, the contribution of theoretical errors accounts for a large proportion of possible differences in the comparison between simulation results and real experiments.

In this study, several functions were used to define material properties which were numerically analysed in order to reduce the error between numerical simulations and actual conditions. The finite element method of COMSOL Multiphysics was used to perform simulation solutions based on fixed chamber pressure, hot filaments power, and gas flow. The combined effects of three heat transfer mechanisms were considered in the simulation process, including solid heat transfer, fluid heat transfer and surface radiation heat transfer. The comprehensive influence of filament arrangement on the temperature distribution of the substrate was studied by multi-physics coupling. Furthermore, an orthogonal experiment was designed to optimize the preparation process by changing three parameters, including the number of filaments (**N**), the distance between the filament and the substrate (**H**), and the separation between two adjacent hot filaments (**S**). Moreover, five Si_3N_4 substrate diamond-coated samples were prepared and characterized by scanning electron microscopy (SEM) and by Raman spectroscopy, which further verified the validity of the simulation results and of the deposition optimization process.

2. Model and simulation of HFCVD system

The simulation model used in this study is displayed in figure 1. The diameter of each filament (Tantalum) is 0.5 mm and the length is 220 mm. The filaments are placed horizontally and equidistantly above the substrate. The number of filaments will be hereinafter specified as N, while the distance between adjacent filaments is marked as S. The distance between the filaments and the upper surface of the Si_3N_4 ceramic substrate is specified as H. The considered substrate is a pressureless sintered Si_3N_4 ceramic square sheet ($x \times y \times z = 20$ mm $\times$ 20 mm $\times$ 2 mm) placed on a horizontal graphite holder with a diameter of 160 mm and a thickness of 20 mm. The contact pressure between the substrate and the graphite holder is 64.5 Pa and the contact surface roughness of both is $Ra = 0.8\ \mu$m. The worktable, whose contact pressure with the graphite holder is 360 Pa, has a diameter of 160 mm and a height of 30 mm, while the surface roughness is $Ra = 2.2\ \mu$m. The cooling channels inside of the worktable are 140 mm in diameter, with forced convection water cooling, and the water temperature is set to a constant temperature of 20 °C and the flow velocity of 0.0035 m/ s^{-1}. The outer wall of the chamber is also cooled by forced convection water at 20 °C, and the water flow velocity of the outer wall surface is 0.002 m/ s^{-1}. The outer wall material of the chamber is stainless steel. The convective heat transfer coefficient database in the software is used to calculate the above water-cooling area, which can ensure that the convective heat transfer occurs on the wall while avoiding calculating the cooling water velocity and pressure field of the two cooling regions, thereby reducing the amount of calculation. The reactive gas is introduced from the upper gas distribution plate and flows out from the lower gas outlet. Finally, boundary layer

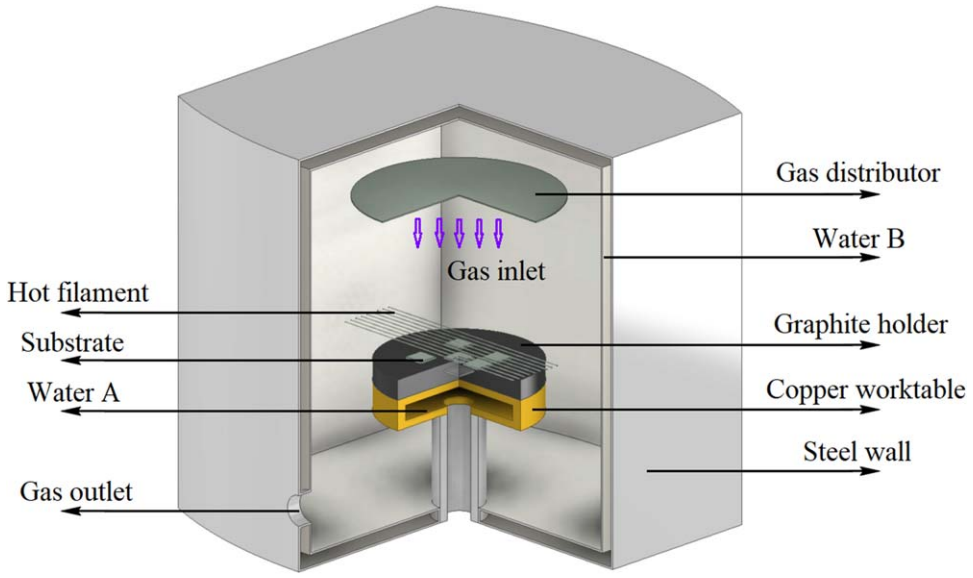

Figure 1. Schematic diagram of HFCVD system 3D model.

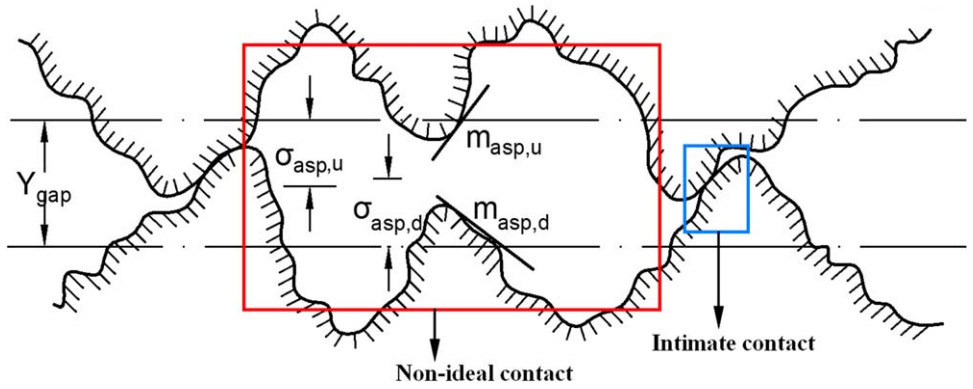

Figure 2. Physical contact at the microscopic level.

and refined solid mesh are added to improve calculation accuracy. The information of the mesh model is as follows: 736919 units, minimum quality 0.12, average quality 0.77.

The contact thermal resistance between the substrate and the graphite holder will greatly affect its heat transfer efficiency. When the two material surfaces are in contact, only a limited number of contact points on the two surfaces will produce solid to solid heat transfer [20], as shown in figure 2.

The presence of roughness will cause the presence of gas in the gap between the contact surfaces. The thermal conductivity of the gas is much lower than that of the solid material. Therefore, the increase in the thermal resistance of the heat flux in the solid areas that are not in contact with each other (non-ideal contact area) will cause the heat flux to decrease. The non-ideal contact area also includes fluid heat transfer and radiation heat transfer between two contact surfaces. The thermal contact boundary is controlled by defining the constriction conductance h_c of the contact surface, the gap conductance h_g, and the radiative conductance h_r; The thermal contact governing equation is as follows:

$$-\vec{n}_d \cdot (-k_d \nabla T_d) = -h(T_u - T_d) \tag{1}$$

$$-\vec{n}_u \cdot (-k_u \nabla T_u) = -h(T_d - T_u) \tag{2}$$

$$h = h_c + h_g + h_r \tag{3}$$

Where $\vec{n}_u$ and $\vec{n}_d$ are the normal vectors on the upper and lower sides of the contact surface, respectively; k_u and k_d are the thermal conductivity of the upper and the lower side, respectively; T_u and T_d represent the temperature of the upper side and the lower side, respectively; h is the total heat transfer coefficient, which is determined by the constriction conductance h_c, the gap conductance h_g and the radiative conductance h_r.

Here, h_c is the Cooper-Mikic-Yovanovich (CMY) thermo-elastoplastic contact model [21–23]. The CMY model is related to the surface roughness and pressure load of the contact surface, and the boundary condition h_c has the following form:

$$h_c = 1.25\frac{2k_u k_d}{k_u + k_d} \times \frac{m_{asp}}{\sigma_{asp}} \times \left(\frac{P}{H_c}\right)^{0.95} \tag{4}$$

Where m_{asp} and σ_{asp} are the average slope of the roughness and the average height of the roughness [24], respectively; p is the contact pressure, H_c is the microhardness of the graphite.

The correlation of gas gap of parallel plates defines h_g by:

$$h_g = \frac{2k_{gap}}{2Y_{gap} + \alpha\beta\frac{\sigma(T_u + T_d)}{2\sqrt{2}\,\pi D^2 p_g}} \tag{5}$$

Where K_{gap} is the parallel-plate gap gas thermal conductivity, Y_{gap} is parallel-plate gap mean separation thickness (equation (6)), which is a function of pressure and microhardness and roughness, meaning that a reduction of Y_{gap} to 0 is considered perfect contact. α is the gas thermal accommodation parameter [25], β is the gas property parameter (equation (7)), σ is the Boltzmann's constant, D is the average gas particle diameter, p_g is the gas environment pressure.

$$Y_{gap} = 1.185\sigma_{asp}\left[-\ln\left(3.132\frac{P}{H_c}\right)\right]^{0.547} \tag{6}$$

$$\beta = \frac{2\gamma}{(\gamma + 1)Pr} \tag{7}$$

Where γ is the specific heat ratio, Pr is the Prandtl number.

At high temperatures above 600 °C the radiative conductivity needs to be considered and the equation is defined as follows:

$$h_r = \frac{\varepsilon_u \varepsilon_d}{\varepsilon_u + \varepsilon_d - \varepsilon_u \varepsilon_d}\sigma(T_u^3 + T_u^2 T_d + T_u T_d^2 + T_d^3) \tag{8}$$

Where ε_u and ε_d are the surface emissivity of Si_3N_4 and graphite, respectively.

The governing equation used for nonisothermal flow in the numerical simulation of HFCVD is the energy conservation equation (generalized heat transfer equation) as follows [26, 27]:

$$\nabla \cdot (-k\nabla T) = Q - \rho C_p \vec{v} \cdot \nabla T + \tau : S - \frac{T}{\rho}\left(\frac{\partial \rho}{\partial T}\right)|_P(\vec{v} \cdot \nabla p) \tag{9}$$

$$\tau = 2\mu S - \frac{2}{3}\mu(\nabla \cdot \vec{v})I \tag{10}$$

$$S = \frac{1}{2}(\nabla\vec{v} + (\nabla\vec{v})^T) \tag{11}$$

The Navier–Stokes equation is used in fluid flow. The N-S equation must be solved simultaneously with the continuity equation, and the continuity equation represents conservation of mass:

$$\nabla \cdot (\rho\vec{v}) = 0 \tag{12}$$

Momentum conservation equation:

$$\rho(\vec{v} \cdot \nabla)\vec{v} = \nabla[-p\mathrm{I} + \tau] + \vec{F} + \rho\vec{g} \tag{13}$$

Where k is the thermal conductivity, T is the temperature, Q is a heat source including viscous dissipation, ρ is the density, C_p is the heat capacity, $\vec{v}$ is the velocity vector, p is the pressure, μ is the dynamic viscosity, $\vec{F}$ is the body force vector, $\vec{g}$ is the gravitational acceleration vector.

Reynolds number 'Re' is the criterion to distinguish laminar flow from turbulent flow. $\mathrm{Re} = \rho vL/u$ is the ratio of inertial force to viscous force. The calculated Reynolds number of hydrogen flow is less than 2100, thus it is considered as laminar flow. When calculating the fluid motion, considering that high temperature filaments and chamber pressure will impact a significant change in the properties of hydrogen, the fluid is defined as a compressible flow [28, 29].

The radiation heat transfer equation in the model is as follows:

$$q = (1 - \rho_d) \cdot G - \varepsilon n^2 \sigma T^4 \tag{14}$$

Where q is the heat flux, ρ_d is the diffuse reflectivity, G is the surface irradiation, ε is the surface emissivity, n is the refractive index, σ is the Boltzmann's constant, T is the temperature.

Table 1. Material properties at 0 °C and standard atmospheric pressure.

Material	Density [kg/m^3]	Thermal conductivity [W/(m·K)]	Heat capacity [J/(kg·K)]	Emissivity
Tantalum	16774.15	57.46	139.45	0.51 [2200 °C]
Si_3N_4	3290	107.71	652.53	0.9
Graphite	1800	130	710	0.8
Copper	8939.81	386.7	383.02	0.4
Stainless steel	7850	19.1	475	0.1
Hydrogen	0.0837	0.1769	14439.68	N/A
Water	998.24	0.5941	4186.92	N/A

In order to simplify the calculation of the simulation process, the following reasonable simplifications were made to the simulation model:

(I) Since the total content of methane inside the deposition chamber is only 1%, the influence of methane on heat transfer is ignored in the calculation, assuming that the inside of the chamber is entirely filled with hydrogen.

(II) Ignoring the trace chemical heat produced by the chemical reaction between hydrogen and methane, such as hydrogen decomposition reaction, bonding reaction of active groups and carbon-carbon bonding, etching reaction of hydrogen atoms, etc.

(III) It is assumed that the hot filament without electrode contact and support only exchanges heat through hydrogen and surface radiation.

(IV) The spectral absorption ratio of all solids is independent of wavelength in the calculation of thermal radiation. Their absorption is equal to the emissivity and is set as an opaque grey body. The radiative heat transfer of hydrogen medium is ignored.

(V) The thermal conductivity of materials is isotropic.

In the simulation work, the tantalum wire will be highly carbonized and form an abnormally rough surface, so the emissivity of the tantalum wire surface is set to 0.51 (2200 °C) [30–32]. Most of the material properties in the simulation model are defined by reference functions, which are functions of temperature or pressure. Table 1 shows several material parameters at 0 °C and standard atmospheric pressure [33, 34].

3. Results and discussions

3.1. Verification of model deviation

The model presented herein was verified by actual temperature measurements, to evaluate its accuracy. The parameters in this actual experiment were as follows: the hydrogen flow rate was 800 sccm, the absolute pressure in the chamber was fixed to 3.0 kPa, a total of 10 tantalum filaments with a diameter of 0.5 mm were used (therefor N = 10; while H = 8 mm and S = 7 mm). The positioning of the substrate plates and the tantalum filaments is shown in figure 3. Five Si_3N_4 ceramic substrates are symmetrically arranged with the centre point of the substrate C as the coordinate origin. Therefore, samples A, B, C, D are selected to study the influence of different parameters on the temperature distribution. The blue lines on each substrate represent the baseline of the temperature data points to be measured. During the deposition process of diamond films, the blue lines on the upper surface of the substrate were used to measure the temperature in real time using a Metis M316 infrared thermometer (uncertainty: 0.25% of measured value, emissivity ε: 0.05–1.20, set to the emissivity value from table 1) after the temperature was stabilized (deposition 1 h). Each point was measured 8 times and the average value was taken as the actual temperature value. The temperature of the filament was monitored with a Metis M311 infrared thermometer (uncertainty: 0.3% of measured value, emissivity ε: 0.05–1.20, set to the emissivity value from table 1) and the applied power on the filament was adjusted to obtain a temperature of 2200 °C. The emissivity ε of tantalum and Si_3N_4 is shown in table 1.

The temperature field distribution of the substrate is shown in figure 4 and the simulation and actual measurement results are shown in figure 5(a) for substrates A, C, and B (x axis—perpendicular to the Ta filaments), and figure 5(b), for substrates A, C, and D (y axis—parallel to the Ta filaments). The temperature at the outer edge of the substrate A in the x-direction is lower, but it gradually increases towards the interior of the substrate holder. The temperature distribution of the substrate B is mirrored to that of substrate A, and the temperature of the substrate is the lowest at the outer edge in reference to the positioning of the filaments, while

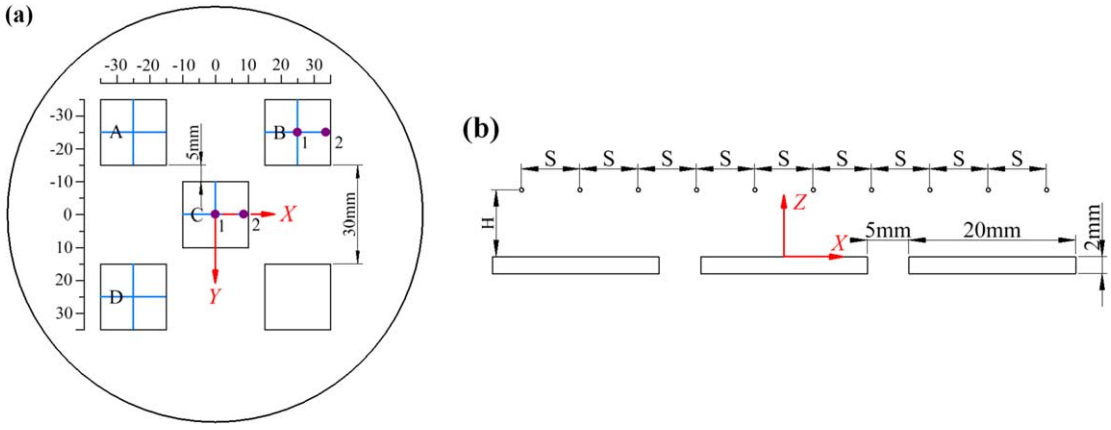

Figure 3. Layout diagram: (a) substrate layout; (b) hot filament layout.

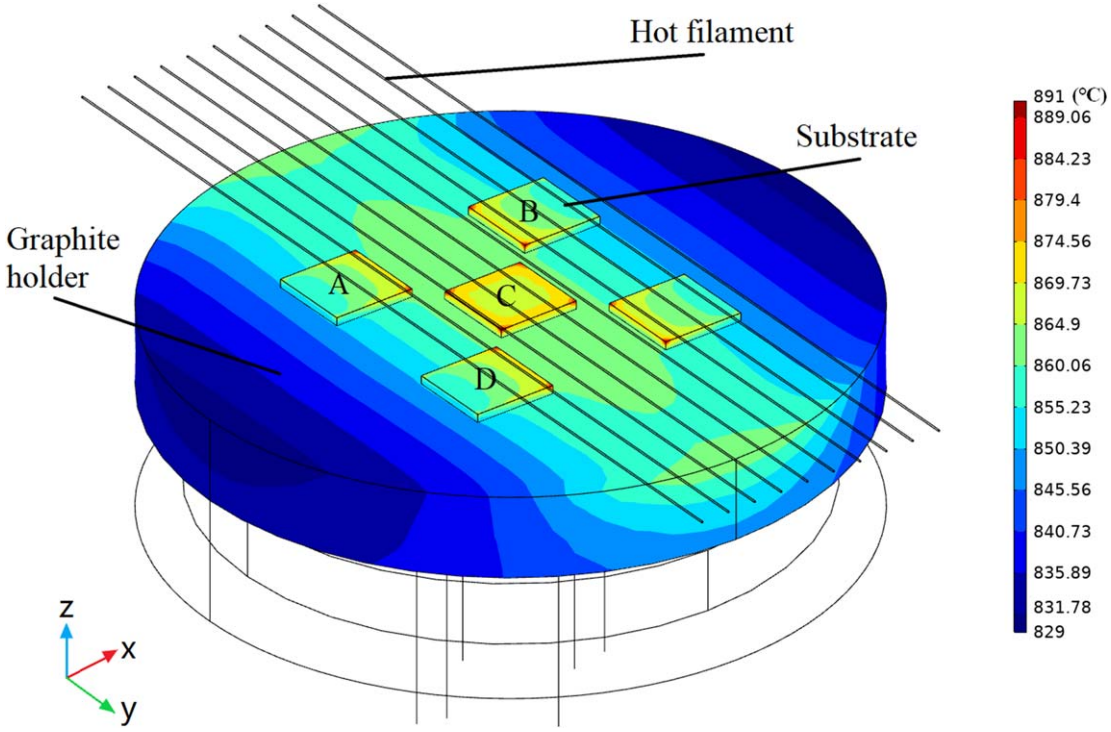

Figure 4. Schematic diagram of substrate temperature field distribution (N = 10, H = 8 mm, S = 7 mm).

the measured maximum temperature difference is $\Delta T_B = 15.5\ ^\circ C$ (*x* axis). This indicates that the heat flux density generated by the outer edges of the A and B substrates is smaller and that the A and B substrates receive less thermal radiation. If the temperature of different substrates is compared in large batch preparation, the temperature difference becomes larger. That is to say, the heat transfer within an individual substrate reduces the temperature difference in the substrate. This phenomenon can be seen by comparing the maximum temperature difference between the experimental temperatures of Zhang *et al* [19] (single substrates) and Wang *et al* [35] (multiple substrates), even though the two experiments were conducted under different preparation conditions. The surface temperature of substrate C presents an arcuate structure, with a higher temperature on both sides and a lower temperature in the middle ($\Delta T_C = 6\ ^\circ C$, *x* axis), which is due to the heat accumulation caused by the difficulty in discharging heat from the edge of the substrate. Comparatively, all three substrates measured on the y-direction (parallel to the Ta filaments), namely A, C, and D, show a trend of low temperature in the middle and high temperature at the edges ($\Delta T_A = 5.6\ ^\circ C$, $\Delta T_C = 7.5\ ^\circ C$, $\Delta T_D = 9\ ^\circ C$, *y* axis). The reason for this phenomenon may be that the side edges have more heat flux in the y-direction compared to other locations thus leading to lateral heat transfer in the side region, which also shows that the temperature distribution in this form is closely related to the thermal contact model of the graphite holder, because the heat

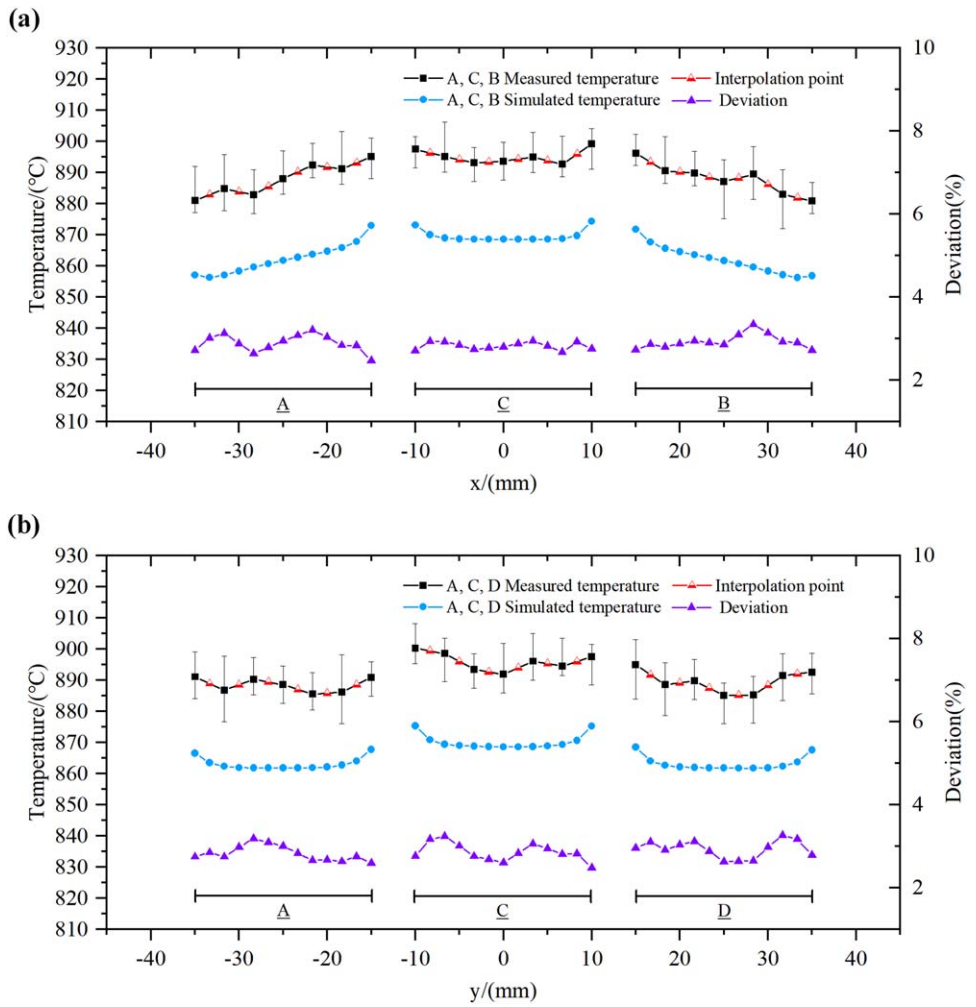

Figure 5. The temperature distribution and deviation of the substrate (N = 10, H = 8 mm, S = 7 mm): (a) the substrate A, C, B in the x-direction; (b) the substrate A, C, D in the y-direction.

absorption in the middle of the graphite holder is stronger, due to the faster cooling of the substrate [19]. The temperature measured in the actual experiment follows essentially the same trend as the simulation, however the measured temperatures are about 26 °C higher. The temperature difference may be due to the combined effect of the micro-chemical heat generated by the polymerization of hydrogen atoms on the surface of the substrate and the carbon-carbon bonding [18], and to possible theoretical errors of the simulation model. However, the temperature difference between the experiment and the simulation is around 3%, which shows that the accuracy of the simulation model can meet certain requirements and can be used as a benchmark for optimizing the process parameters.

3.2. Optimization of the substrate temperature field

Taguchi orthogonal experiments are a highly efficient design method in which a representative selection of points from a full-scale experiment is selected for the experiment based on orthogonality. Orthogonal simulation experiments are performed by controlling variables. Considering that the pressure during the deposition process, the filament temperature, and the gas flow rate will all affect the temperature of the substrate, they are set to fixed values, in order to investigate the effect of other conditions on the substrate temperature, namely the number of filaments (N), the distance between adjacent filaments (S), and the distance between the filaments and the upper surface of the substrates (H). For each of these three variable parameters (N, H, and S) three values were chosen: N = 9, 10, 11; H = 8, 10, 12 mm; S = 7, 10, 13 mm. The results obtained from nine sets of simulation experiments are shown in table 2: x_{max} and y_{max} are the maximum temperatures in the x and y directions, respectively; x_{min} and y_{min} are the minimum temperatures in the x and y directions, respectively; T_A is the average temperature of the discrete data points of the substrates in the x and y directions measured in each set of experiments, its statistical method is to calculate the total average of the temperature data of substrates A, C and B in x direction plus substrates A, C and D in y direction; σ_x and σ_y are the standard deviations of x and y

Table 2. Orthogonal experimental design.

No.	Filament number N	Filament-substrate distance H (mm)	Filament-filament distance S (mm)	x_{max}	x_{min}	y_{max}	y_{min}	T_A	σ_x	σ_y
1	9	8	7	846.5	826.2	848.1	833.6	837.0	6.1	4.3
2	9	10	10	840.3	830.2	840.6	831.9	834.0	2.6	2.3
3	9	12	13	829.9	822.6	829.7	823.4	824.9	1.8	1.6
4	10	8	10	894.1	882.4	893.7	885.0	887.0	2.8	2.3
5	10	10	13	875.6	868.0	875.8	869.8	870.9	1.9	1.5
6	10	12	7	823.0	809.4	823.5	813.4	816.0	4.0	3.0
7	11	8	13	923.0	915.5	923.6	916.2	917.8	1.8	1.8
8	11	10	7	869.1	856.3	870.6	859.8	862.4	3.8	3.1
9	11	12	10	864.7	856.8	865.6	857.7	859.5	2.0	1.9

direction, respectively. It can be seen from table 2 that No.7 has the highest average temperature and the temperature value reaches 917.8 °C. As expected, increasing the number of filaments and reducing the distance between the filaments and the substrate can significantly increase the surface temperature of the substrate. In our previous experience, the equipment used for real life verification of the model (section 3.3) can deposit high quality diamond films on Si_3N_4 substrates heated at 900 °C–920 °C, so the goal of optimizing the preparation parameters is to obtain a smaller temperature standard deviation σ in this temperature range, so as to avoid the occurrence of inhomogeneity in the deposited films. Moreover, configuration No.6, which has the lowest S value (distance between filaments), but the highest distance between the filament and the substrate, results in the lowest average temperature, due to less thermal radiation received by the substrates. In addition, the small spacing of the filaments may also cause the temperature distribution in the hot filament area to be more concentrated. Furthermore, the small spacing of the filaments might indirectly cause the convective heat flux of hydrogen passing through the filaments area to be smaller than the heat flux when the distance between the filaments is larger.

Figures 6(a) and (b) exhibit the temperature distribution curves calculated for the x-direction (substrates A, C, and B) and for the y-direction (substrates A, C, and D). One can observe that the temperature difference between the substrates from the same axis decreases with the increase of the average temperature, for both x and y directions. When the overall average temperature is lower (for example conditions No.6 or No.1), the temperatures calculated for the x-direction on the outer edge of the A and B substrates is lower than that of the center of the substrate. This phenomenon is not observed in the y-direction, which indicates that in order to obtain a more uniform temperature distribution, the problem of poor temperature uniformity in the x-direction must be solved.

Figures 7(a) and (b) contain the standard deviation x-σ of substrates A, C, and B in the x-direction and the standard deviation y-σ of substrates A, C, and D in the y-direction, as function of the variable parameters (N, H, and S). The standard deviation σ in the x-direction gradually decreases with the increase of N, which signifies that increasing the number of filaments can effectively reduce the temperature difference of the substrate, thus potentially improving the uniformity of the diamond film. Furthermore, the standard deviation decreases rapidly when H increases from 8 mm to 10 mm, followed by a gentler downward slope when H increases from 10 mm to 12 mm. It can be understood that when the H value is smaller, the temperature isosurface produces a larger temperature gradient on the substrate in a small area, and the temperature distribution becomes uneven. As the value of H increases, the distribution range of the isosurface of the temperature around the filament becomes larger and smoother, so the standard deviation σ has a decreasing trend. The standard deviation σ in the x-direction decreases with the increase of the filaments spacing S, which results in a more uniform distribution of the surrounding temperature field due to the larger heating area. There is no significant decrease in the standard deviation σ in the y-direction when N is equal to 10 or 11, as presented in figure 7(b), which indicates that the temperature gradient generated in the hot filament direction becomes less sensitive to the number of hot filaments when a certain number of filaments is reached. The influence of H and S on the standard deviation σ is consistent with the one observed for the x-direction. Generally, the influence of N, H, and S variations in the y-direction on the standard deviation σ is smaller than that in the x-direction, which results in more stable heating mechanism. Therefore, the longer side of the workpiece should be kept parallel with the filament direction when depositing the coatings, to obtain uniform characteristics.

Figure 7(c) shows the influence of the three variable parameters on the substrate average temperature. The N-T_A curve shows that the average temperature increases gradually as N (the number of filaments) increases. The increase of N can be regarded as the increase of radiation source area. The Stefan-Boltzmann's radiation law states that the radiation power per unit area per unit time is proportional to the fourth power of the temperature. Consequently, the increase in the number of the filaments should be beneficial to raise the temperature of the

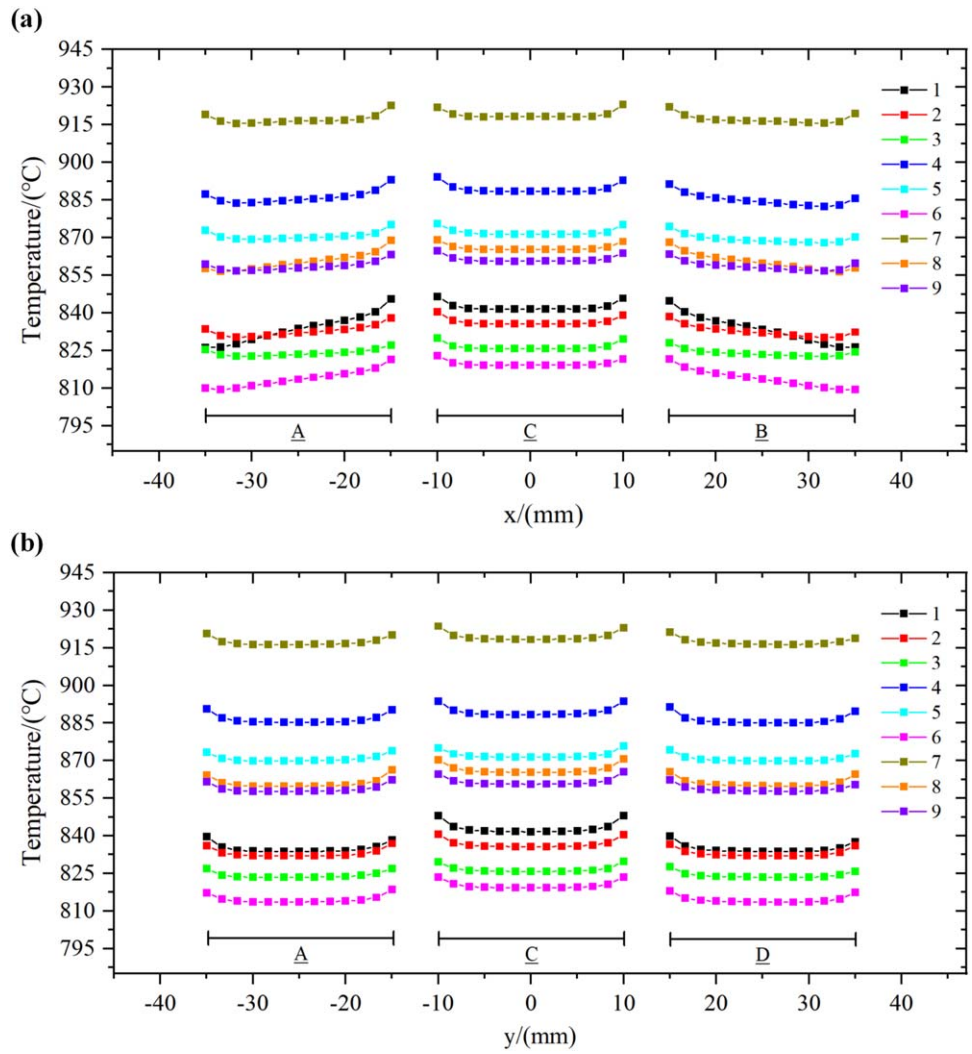

Figure 6. The substrate temperature based on orthogonal experiment was obtained by simulation: (a) the substrate A, C, B in the x-direction; (b) the substrate A, C, D in the y-direction.

substrate. Moreover, it can be seen from the H-T_A curve that the distance between the filaments and the substrate has also a strong influence on the overall temperature of the substrate: a higher temperature is obtained when the distance between the filaments and the substrate is smaller. The temperature of the substrate drops rapidly when H increases. Therefore, the distance between the filaments and the substrate can be unilaterally controlled to adjust the overall temperature of the substrate during deposition. According to the S-T_A curve, the temperature gradually increases when the S spacing increases. This phenomenon differs from the results observed by Liu *et al* [36], and we suppose that the variation of the S parameter has an inflection point that coincides with the maximum average temperature of the substrate, so the effect of S on the average temperature of the substrate is not just linear increase or decrease. This phenomenon could be explained by the following two reasons: (I) the increase in the spacing between the hot filaments leads to more heat carried by the unit hydrogen from the area of the hot filament, so the contribution of the fluid-solid heat transfer increases, resulting in a higher total convective heat transfer coefficient; (II) the increased spacing of the hot filaments leads to an increase in the temperature of the graphite holder and an increase in the uniformly heated area, which in turn causes the transfer of heat from the graphite table to the substrate. When the S parameter was increased to 16 mm (results not shown herein), this trend disappeared, possibly due to the fact that the thermal radiation effect of multiple filaments per unit area gradually weakened, leading to a decrease in the temperature of the substrate.

Based on these results and observations, the influence of these three parameters on the substrate temperature and the standard deviation σ were calculated. The influence law on the average temperature T_A is H > N > S, while the influence law on the standard deviation σ is S > H > N. According to these results, the standard deviation σ decreases with the increase of N, so the optimal hot filament number N was chosen as 11, for a temperature range for the preparation between 900 °C–920 °C. Furthermore, since the H value between 10 mm

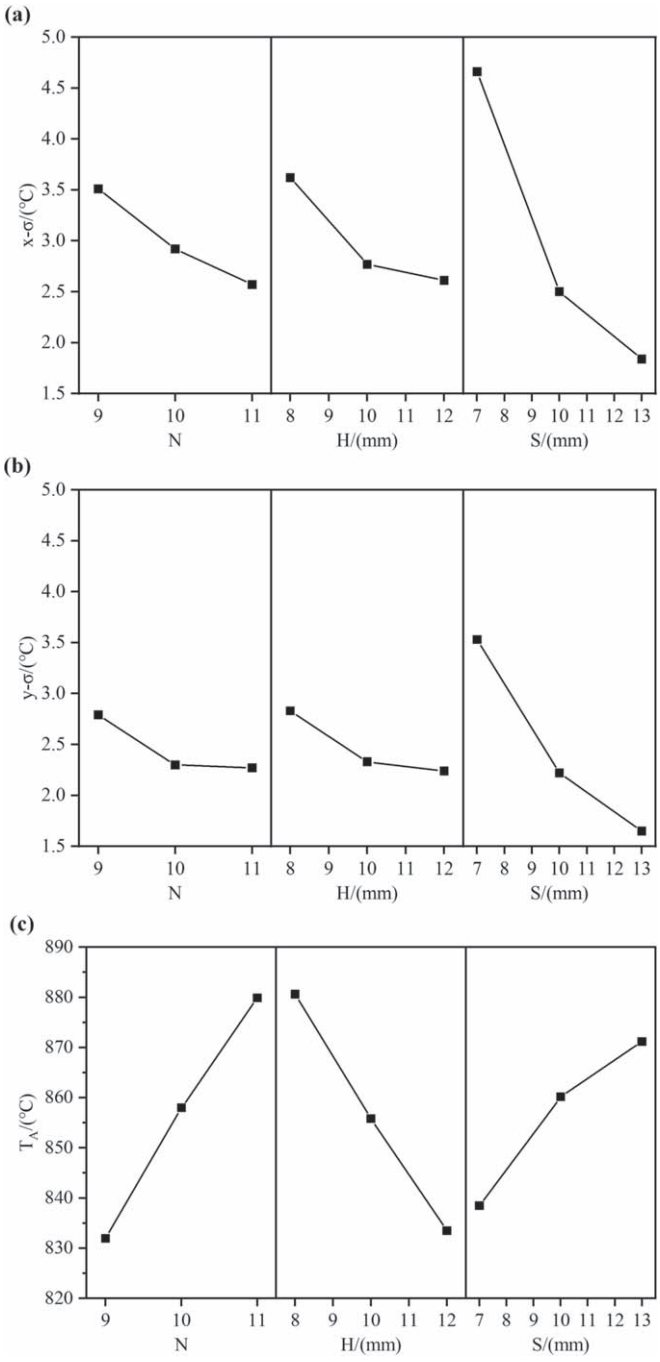

Figure 7. Effect of three parameters on substrate temperature and standard deviation: (a) the standard deviation σ of the substrates A, C, B in the x-direction; (b) the standard deviation σ of the substrates A, C, D in the y-direction; (c) the average temperature of substrate A, B, C, D in the x-y direction.

and 11 mm does not have a significant effect on the standard deviation σ, but has the strongest effect on the average temperature, H was chosen to be 10 mm as the main parameter for regulating the temperature. The standard deviation σ of S is reduced when S is chosen as 13 mm compared to S as 10 mm, but S $=$ 10 mm was chosen as the preferred parameter in consideration of the increase in temperature. Therefore, N $=$ 11, H $=$ 10 mm, and S $=$ 10 mm were determined as the optimal parameters for subsequent experiments, which should contribute to a good temperature uniformity and a suitable temperature range.

3.3. Verification of optimized parameters

The deposition of diamond coatings onto Si_3N_4 substrates was carried out according to the optimized parameters resulted from simulations (N $=$ 11, H $=$ 10 mm, S $=$ 10 mm). The reaction pressure was set to 3.0 kPa. The flow rates of hydrogen and methane were set to 800 sccm and 8 sccm, respectively. The filament power was set to 3.2 $\pm$ 0.2 KW (to reach a temperature of 2200 °C). The substrates (Si_3N_4 - surface roughness Ra $=$ 0.8

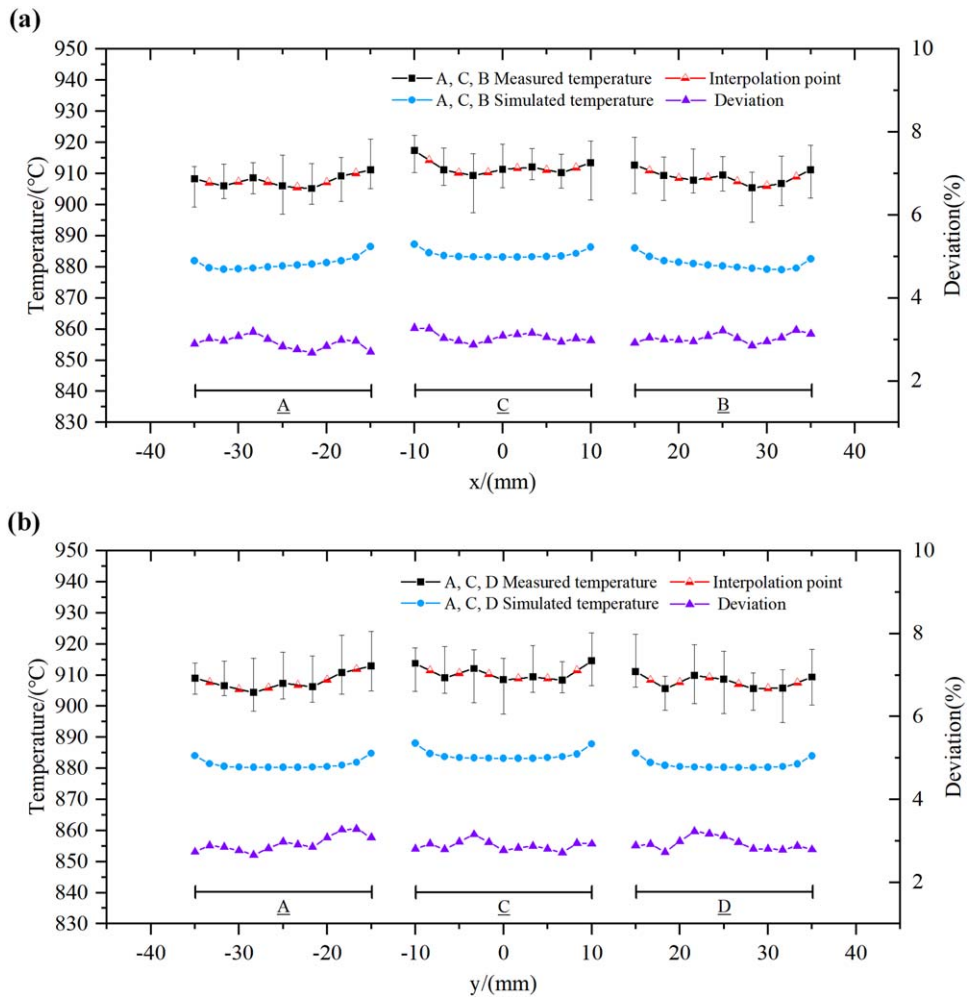

Figure 8. The substrate temperature distribution and deviation obtained after optimization (N = 11, H = 10 mm, S = 10 mm): (a) the substrate A, C, B in the x-direction; (b) the substrate A, C, D in the y-direction.

μm) were degreased with acetone for 20 min in an ultrasonic bath, followed by surface etching for 2 min in 40% HF solution, in order to remove the natural oxide layer and to increase the roughness. Furthermore, the substrates were treated to ultrasonic vibration in diamond powder suspension (diamond particles 3.7 $\pm$ 0.7 nm) for 15 min, in order to improve the nucleation density. The treated substrates were ultrasonically cleaned with deionized water for 10 min to remove excess diamond particles on the surface, followed by nitrogen blowing. The deposition stage was carried out for 3 h.

The variation of the substrate surface temperature as function of position and measuring direction, while applying the optimized parameters, is shown in figures 8(a) and (b). One can observe that the temperatures measured in the x-direction become more stable, and that the previous situation of low temperatures at the outer edges of substrates A and B has improved considerably ($\Delta T_A = 5.9\,^{\circ}C$, $\Delta T_C = 8\,^{\circ}C$, $\Delta T_B = 7.3\,^{\circ}C$, x axis). The measurement results are highly consistent with the simulation temperature trend, and the deviation is about 2.9%.

Figure 9 shows the surface morphology of the diamond films at different locations, obtained by field emission scanning electron microscopy (FESEM, Hitachi S-4800). Figures 9(a)–(d) represent the four different locations of the sampling points for substrate B (B_1, B_2) and substrate C (C_1, C_2), respectively, as shown in figure 3. A uniform microcrystalline diamond film is present on the surfaces of the B and C substrates, which is continuous and dense. The diamond crystals are about 1–1.5 μm in size, exhibiting a sharp micro-pyramidal morphology. The uniform distribution of the Si_3N_4 substrate surface temperature field after optimizing the preparation parameters leads to similar characteristics of the coatings, regardless of the placement of the substrates on the holder, and the diamond grain growth rate tends to be even for both samples and both analysis positions.

Raman spectroscopy can determine the quality of diamond according to the phonon spectrum of the sample or the Raman shift generated by quasiparticle excited Raman scattering. The Raman spectra of the diamond

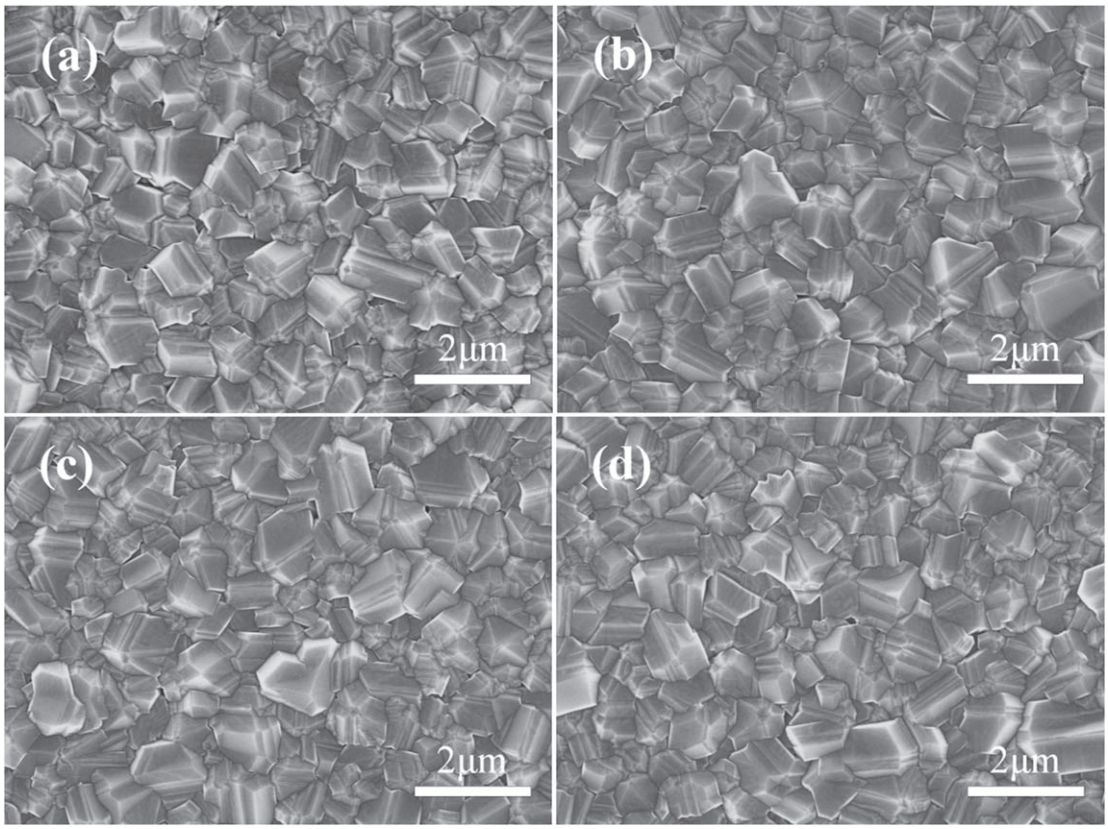

Figure 9. SEM micrographs of diamond films at different positions: (a) B_1; (b) B_2; (c) C_1; (d) C_2.

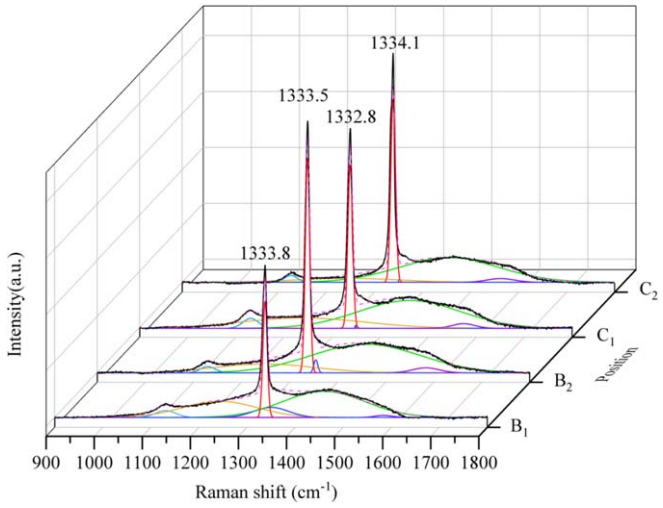

Figure 10. Raman spectra of diamond films at positions B_1, B_2, C_1, C_2.

films are shown in figure 10, and the characteristic peaks of diamond can be observed at 1333.8, 1333.5, 1332.8 and 1334.1 cm^{-1} for the B_1, B_2, C_1 and C_2 points, respectively. Compared with the Raman shift of the natural diamond, located at 1332 cm^{-1}, the position of the characteristic peaks of the four sampling points has a slight shift to the right. The main reason is that the difference in thermal expansion coefficient between Si_3N_4 and diamond leads to the accumulation of residual compressive stress between the film and the substrate. As a result, the diamond grains are slightly deformed and the C–C bond length is shortened, which leads to an increase in atomic vibrations frequency under incident light [37, 38]. The quantitative assessment of residual stresses in diamond films is calculated using the following equation [39]:

$$\sigma_s = -0.567(n - n_0)\,\mathrm{GPa/cm^{-1}} \quad (15)$$

Where n is the measured diamond characteristic peak position and n_0 is the characteristic peak position (1332 cm^{-1}) for an unstressed diamond monocrystal. The residual compressive stress corresponding to B_1, B_2, C_1, and C_2 is −1.021 GPa, −0.851 GPa, −0.454 GPa and −1.191 GPa, respectively. It should be noted that the residual stress of diamond films is composed of thermal stress and intrinsic stress. The thermal stress is caused by the different thermal expansion coefficient of diamond and substrate, and the intrinsic stress is caused by lattice mismatch or diamond growth defects (graphite or non-diamond phase). The peaks situated at 1130 cm^{-1} and 1450 cm^{-1} are characteristic for trans-polyacetylene. Ferrari *et al* [40] attribute these two peaks to the C–C sp^2 vibration of trans-polyacetylene at the grain boundaries, which is caused by the diffusion and aggregation of hydrogen atom in the films. The four sampling points have relatively weak Raman scattering peaks near 1580 cm^{-1}, corresponding to the graphite structure of sp^2 hybrid orbitals. This may be caused by the formation of graphite and amorphous carbon in the grain boundary regions during the deposition process. However, the sensitivity of the sp^2 phase in the Raman spectrum is about 50 times higher than that of the sp^3 phase, thus showing that the diamond phase is dominant in these films [41]. All four sampling points have strong diamond characteristic peaks and narrow peak widths, and the Raman curves are highly consistent. This observation shows that the diamond films prepared by using the simulation optimized parameters have good uniformity and high crystalline quality and purity. In summary, this experiment obtained optimized conditions, suitable for uniform growth of diamond films, by adjusting appropriate deposition parameters, and verified the effectiveness of the simulation optimization results by scanning electron microscopy and Raman spectroscopy, applied to samples deposited using the optimized parameters.

4. Conclusion

The surface temperature distribution of the Si_3N_4 ceramic substrate was solved through the coupling of three heat transfer mechanisms. The orthogonal experiment results show that for the standard deviation σ representing the degree of temperature dispersion, S (spacing between filaments) has the greatest influence, followed by H (distance between filaments and substrate) and N (number of filaments). The law of influence on the average temperature of the substrate is H > N > S. Moreover, the temperature uniformity of the substrate placed along the hot filament direction (y-direction) is significantly better than that in the x-direction, which is caused by a decreased temperature gradient in the filament direction. In addition, all substrates show a situation of high edge temperature and low centre temperature, which is related to the thermal contact between the substrate and the graphite holder.

The optimized parameters of the simulation were verified experimentally (N = 11, H = 10 mm, S = 10 mm), and the temperature curve of the discrete points was highly consistent with the temperature curve obtained from simulation. The deposited diamond film had uniform surface morphology and crystal quality. This study explained the influence of the filament arrangement on the temperature distribution of the substrate, and provided the accurate temperature field distribution, which can be applied to the preparation of large quantities of coated parts.

Acknowledgments

This research was supported by the Programme of Introducing Talents of Discipline to Universities (the 111 program) (No. D18017); National Natural Science Foundation of China (No. 51942507); Shenyang Science and Technology Bureau (No. 18-400-6-05).

Data availability statement

The data that support the findings of this study are available upon reasonable request from the authors.

ORCID iDs

Huisen Zhang https://orcid.org/0000-0002-6790-8473
Guangyu Yan https://orcid.org/0000-0003-3242-5348
Daniel Cristea https://orcid.org/0000-0002-3871-1436

References

[1] Ajikumar P K, Ganesan K, Kumar N, Ravindran T R, Kalavathi S and Kamruddin M 2019 Role of microstructure and structural disorder on tribological properties of polycrystalline diamond films *Appl. Surf. Sci.* **469** 10–7

[2] Yan G *et al* 2019 Mechanical properties and wear behavior of multi-layer diamond films deposited by hot-filament chemical vapor deposition *Appl. Surf. Sci.* **494** 401–11

[3] Lu F, Li H, Zha L, Wang Y, Liu L and Yuan Z 2019 Preparation of diamond-gradient film and analysis of its mechanical properties *Mater. Res. Express* **6** 086441

[4] Motahari H and Malekfar R 2017 Bottom-up diamond nanorod growth in HFCVD from nanocrystalline diamond film as a template-free method *Mater. Res. Express* **4** 075030

[5] Belmonte M, Fernandes A J S, Costa F M, Oliveira F J and Silva R F 2003 Adhesion behaviour assessment on diamond coated silicon nitride by acoustic emission *Diamond Relat. Mater.* **12** 733–7

[6] Abreu C S, Amaral M, Fernandes A J S, Oliveira F J, Silva R F and Gomes J R 2006 Friction and wear performance of HFCVD nanocrystalline diamond coated silicon nitride ceramics *Diamond Relat. Mater.* **15** 739–44

[7] Amaral M, Oliveira F J, Belmonte M, Fernandes A J S, Costa F M and Silva R F 2004 Hot-filament chemical vapour deposition of nanodiamond on silicon nitride substrates *Diamond Relat. Mater.* **13** 643–7

[8] Polini R, Mattei G, Marucci A and Traversa E 1998 Diamond synthesis on silicon nitride by the hot filament chemical vapor deposition technique *J. Ceram. Soc. Jpn.* **1240** 1167–71

[9] Yan G, Wu Y, Cristea D, Lu F, Wang Y, Zhao D, Tierean M and Liu L 2019 Machining performance of hard-brittle materials by multi-layer micro-nano crystalline diamond coated tools *Results Phys.* **13** 102303

[10] Yuan Z, Liu L, Song H, Lu Z, Yang B, Xiong J, Huang N and Jiang X 2021 Improvement in the universality of high-performance CVD diamond coatings on different WC-Co substrates by introducing multilayered diamond/β-SiC composite *Diamond Relat. Mater.* **116** 108369

[11] Kumar N, Sankaran K J, Kozakov A T, Sidashov A V, Nicolskii A V, Haenen K and Kolesnikov V I 2019 Surface and bulk phase analysis of the tribolayer of nanocrystalline diamond films sliding against steel balls *Diamond Relat. Mater.* **97** 107472

[12] Comerford D W, Smith J A, Ashfold M N and Mankelevich Y A 2009 On the mechanism of H atom production in hot filament activated H 2 and CH 4/H 2 gas mixtures *J. Chem. Phys.* **131** 044326

[13] Joshi P, Haque A, Gupta S, Narayan R J and Narayan J 2021 Synthesis of multifunctional microdiamonds on stainless steel substrates by chemical vapor deposition *Carbon* **171** 739–49

[14] Song G H, Yoon J H, Kim H S, Sun C, Huang R F and Wen L S 2002 Influence of hot filaments arranging on substrate temperature during HFCVD of diamond films *Mater. Lett.* **56** 832–7

[15] Song G H, Sun C, Huang R F, Wen L S and Shi C X 2000 Heat transfer simulation of HFCVD and fundamentals of diamond vapor growth reactor designing *Surf. Coat. Technol.* **131** 500–5

[16] Song C W, Lee Y H, Heo S Y, Hwang N M, Choi S and Kim K H 2018 Computer simulation of temperature parameter for diamond formation by using hot-filament chemical vapor deposition *Coatings.* **8** 15

[17] Wang X, Zhang T, Shen B, Zhang J and Sun F 2013 Simulation and experimental research on the substrate temperature distribution in HFCVD diamond film growth on the inner hole surface *Surf. Coat. Technol.* **219** 109–18

[18] Shen B, Song B, Cheng L, Lei X and Sun F 2014 Optimization on the HFCVD setup for the mass-production of diamond-coated micro-tools based on the FVM temperature simulation *Surf. Coat. Technol.* **253** 123–31

[19] Zhang T, Zhang J, Shen B and Sun F 2012 Simulation of temperature and gas density field distribution in diamond films growth on silicon wafer by hot filament CVD *J. Cryst. Growth* **343** 55–61

[20] Grujicic M, Zhao C L and Dusel E C 2005 The effect of thermal contact resistance on heat management in the electronic packaging *Appl. Surf. Sci.* **246** 290–302

[21] Bergman T L, Incropera F P, Lavine A S and Dewitt D P 2011 *Introduction to Heat Transfer.* (New York: Wiley) (http://refhub.elsevier.com/S2211-2855(17)30226-4/sbref30)

[22] Ji C, Zhu H and Jiang W 2013 Fractal prediction model of thermal contact conductance of rough surfaces *Chin. J. Mech. Eng.* **26** 128–36

[23] Yovanovich M M 2005 Four decades of research on thermal contact, gap, and joint resistance in microelectronics *IEEE Trans. Compon. Packag. Technol.* **28** 182–206

[24] Yüncü H 2006 Thermal contact conductance of nominaly flat surfaces *Heat Mass Transfer* **43** 1–5

[25] Song S, Yovanovich M M and Nho K 1992 Thermal gap conductance-Effects of gas pressure and mechanical load *J. Thermophys. Heat Transfer* **6.1** 62–8

[26] Kaviany M 2013 *Principles of Convective Heat Transfer.* (New York: Springer)

[27] Modest M F 2013 *Radiative Heat Transfer.* (New York: Academic)

[28] Massarotti N, Nithiarasu P, Codina R, Principe J and Ávila M 2010 Finite element approximation of turbulent thermally coupled incompressible flows with numerical sub-grid scale modelling *Int. J. Numer. Methods Heat Fluid Flow* **20** 492–515

[29] Lee D H, Park H J and Ligrani P 2012 Milliscale confined impinging slot jets: Laminar heat transfer characteristics for an isothermal flat plate *Int. J. Heat Mass Transfer* **55** 2249–60

[30] Milošević N D, Vuković G S, Pavičić D Z and Maglić K D 1999 Thermal properties of tantalum between 300 and 2300 K *Int. J. Thermophys.* **20** 1129–36

[31] Malter L and Langmuir D B 1939 Resistance, emissivities and melting point of tantalum *Phys. Rev.* **55** 743

[32] Eckstein B H and Forman R 1962 Preparation and some properties of tantalum carbide *J. Appl. Phys.* **33** 82–7

[33] Zhao Z N 2005 *Heat Transfer (Chinese print)* (Beijing: Higher Education Publisher)

[34] Touloukian Y S 1970 *Thermal Radiative Properties: Metallic Elements and Alloys* (New York: IFI/Plenum)

[35] Wang H, Shen X, Wang X and Sun F 2020 Simulation and experimental researches on the substrate temperature distribution of the large-capacity HFCVD setup for mass-production of diamond coated milling tools *Diamond Relat. Mater.* **101** 107610

[36] Liu J, Wang L, Zhang J, Shen B and Sun F 2016 Simulation of temperature distribution in hot filament chemical vapor deposition diamond films growth on SiC seals *Shanghai Jiaotong Univ. (Sci.).* **21** 541–7

[37] McNamara D, Alveen P, Damm S, Carolan D, Rice J H, Murphy N, Ivanković A and Raman A 2015 spectroscopy investigation into the influence of thermal treatments on the residual stress of polycrystalline diamond *Int. J. Refract. Met, Hard Mater.* **52** 114–22

[38] Gries T, Vandenbulcke L, Simon P and Canizares A 2007 Stresses in textured and polycrystalline cubic films by Raman spectroscopy: Application to diamond *J. Appl. Phys.* **102** 083519

[39] Fan Q H, Gracio J and Pereira E 2000 E, Evaluation of residual stresses in chemical-vapor-deposited diamond films *J. Appl. Phys.* **87** 2880–4

[40] Ferrari A C and Robertson J 2001 Resonant Raman spectroscopy of disordered, amorphous, and diamondlike carbon *Phys. Rev. B* **64** 075414
[41] Sharda T, Rahaman M M, Nukaya Y, Soga T, Jimbo T and Umeno M 2001 Structural and optical properties of diamond and nano-diamond films grown by microwave plasma chemical vapor deposition *Diamond Relat. Mater.* **10** 561–7